

CrystEngComm

Accepted Manuscript



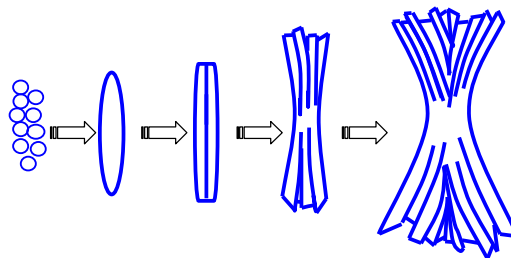
This is an *Accepted Manuscript*, which has been through the Royal Society of Chemistry peer review process and has been accepted for publication.

Accepted Manuscripts are published online shortly after acceptance, before technical editing, formatting and proof reading. Using this free service, authors can make their results available to the community, in citable form, before we publish the edited article. We will replace this *Accepted Manuscript* with the edited and formatted *Advance Article* as soon as it is available.

You can find more information about *Accepted Manuscripts* in the [Information for Authors](#).

Please note that technical editing may introduce minor changes to the text and/or graphics, which may alter content. The journal's standard [Terms & Conditions](#) and the [Ethical guidelines](#) still apply. In no event shall the Royal Society of Chemistry be held responsible for any errors or omissions in this *Accepted Manuscript* or any consequences arising from the use of any information it contains.

Table of Contents Entry



Novel CuO straw sheaves formed by splitting growth show an improved photodegradation activity of RhB.

Cite this: DOI: 10.1039/c0xx00000x

www.rsc.org/xxxxxx

ARTICLE

Splitting growth of novel CuO straw sheaves and the improved photocatalytic activity by active {110} facets exposed and crystallinity

Yunxuan Zhao, Huaxia Shi, Mingdong Chen and Fei Teng*

Received (in XXX, XXX) Xth XXXXXXXXX 20XX, Accepted Xth XXXXXXXXX 20XX

5 DOI: 10.1039/b000000x

In this paper, the novel straw sheaf-like CuO single crystals have been, for the first time, prepared through a facile two-step process: hydrothermal and subsequent calcination. We have mainly investigated the influences of the copper (II) concentration, the added amount of hexamethylenetetramine (HMT), reaction temperature and time on the samples. The samples are characterized by X-ray diffraction (XRD), scanning electron microscopy (SEM), high-resolution transmission electron microscopy (HRTEM) and nitrogen sorption
10 isotherms. The results show that the formed CuO straw sheaves are fairly uniform, and the single straw grows preferentially along the [001] orientation. It is proposed that the CuO straw sheaves form by crystal splitting growth. Furthermore, under visible-light irradiation, the CuO straw sheaves exhibit 5.3 times as high as the irregular sample for the degradation of rhodamine B (RhB), which has been ascribed to the exposed {110} facets and high crystallinity.

Cite this: DOI: 10.1039/c0xx00000x

www.rsc.org/xxxxxx

ARTICLE

1. Introduction

Over the recent years, various nanostructures from one-dimensional (1D) to three-dimensional (3D) hierarchical architectures [1-6] have been intensively studied due to their potential applications in light-emission/detection, field emission, biomedical devices, gas sensors, battery electrodes, and so on. To date, incredible efforts have been made to develop new methods to fabricate new hierarchical architectures [6,7]. However, it is still a big challenge to develop a facile, environmentally friendly, low-cost method for the synthesis of highly-uniform hierarchical micro/nanostructures without using any catalysts and surfactants.

Copper Oxide (CuO), as a p-type semiconductor with a narrow band gap of 1.2 eV has been widely applied in photocatalysts [8-10], gas sensors [11], cathode materials [12-14], and so on. Fascinated by the preeminent properties and wide applications of CuO nanomaterials, various CuO nanostructures including cubes [15,16], polyhedrons [17,18], wires [19-21], prisms [22] and rods [23-26], nanofibers [27], nanoribbons [28,29] have been prepared. In particular, 2D and 3D CuO nanostructures have attracted significant interest of material scientists' due to the fascinating physicochemical properties. Herein, novel CuO straw sheaves are, for the first time, prepared without employing any surfactants or catalysts. The straw sheaves form via an interesting crystal splitting mechanism, which is similar to that of mineral crystals in nature. It is found that the straw grows preferentially along the [001] direction. Moreover, these CuO straw sheaves exhibit a high photocatalytic activity for rhodamine B (RhB) under visible-light irradiation.

2. Experiment section

2.1 Chemicals and materials

All chemicals, copper sulfate (CuSO₄), sodium hydroxide (NaOH) and hexamethylenetetramine (HMT), were analytical reagent and used as received without further purification.

2.2 Preparation of the samples

Preparation of CuO straw sheaves. Typically, 20 mL of 0.5M NaOH solution was added into 20 mL of 0.785 M CuSO₄ (15.7mmole) solution under stirring. Subsequently, 50 mmol of HMT was added to the above mixture. After stirring 10 minutes, the mixture was transferred into a Teflon-lined stainless steel autoclave and maintained at 120 °C for 24 h. After the autoclave was cooled to room temperature naturally, the light green product was harvested by centrifugation, washed with deionized water for several times, and dried at 60 °C for 6 h. Finally, the dried powders were calcined at 500 °C for 1 h in a muffle.

Preparation of irregular CuO. Typically, 40 mL of 0.5 M NaOH was directly added into 20 mL of 0.785 M CuSO₄ solution under stirring and a blue precipitate was produced immediately. Subsequently, the above mixture was transferred into a 60-mL

Teflon-lined stainless steel autoclave and then maintained at 120 °C for 20 h. The product was obtained using the similar procedure as above. After the autoclave was cooled to room temperature naturally. The black product was harvested by centrifugation, washed with deionized water several times, and then dried in air at 60 °C for 6 h.

2.3 Characterization

The size and morphology of the sample were examined by a scanning electron microscopy (SEM, Hitachi SU1510), and a high-resolution transmission electron microscopy (HRTEM, JEOL-2010) equipped with selected area electron diffraction (SAED). The crystal phase and crystallinity of the sample were characterized by a X-ray diffraction (XRD, BRUKER D8) using Cu K_α radiation ($\lambda = 0.154$ nm) in the range of 10-80°. The surface area of the sample was measured by using N₂ physico adsorption isotherm on a Micrometrics Tristar II 3020; and the UV-vis diffusion reflection spectrum was performed on Spectrumlab 722sp spectrophotometer at room temperature. Nitrogen adsorption-desorption isotherms were performed at 77 K on the Autosorb-iQ physicoadsorption apparatus (Quantachrome). Super cells of CuO crystals by Material Studios softwares.

2.4 Photocatalytic activity measurements

The photocatalytic activities of the samples were evaluated by the degradation of RhB dye under visible light ($\lambda \geq 420$ nm), using a 500 W Xe arc lamp (CEL-HXF 300) equipped with an ultraviolet cutoff filter as a light source. The reaction system was placed in a sealed black box with the top opened, and was maintained a distance of 15 cm from the light source. The photocatalysts (100 mg) were dispersed in 200 mL of 1 mg/L RhB aqueous solution in a Pyrex beaker at room temperature. Before lamp was turned on, the suspension was continuously stirred for 30 min in the dark to ensure the establishment of an adsorption-desorption equilibrium between the catalyst and RhB. During degradation, 3 mL of solution was collected by pipette at an intervals of irradiation, and subsequently centrifuged to remove the catalysts. UV-vis spectra were recorded on a Spectrumlab 722sp spectrophotometer to determine the concentration of RhB.

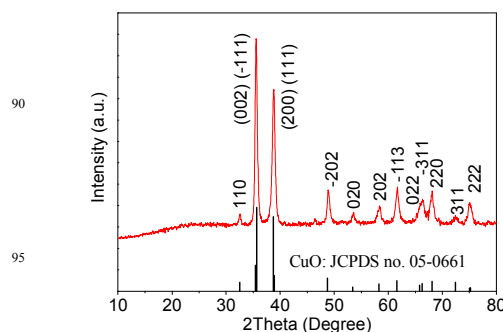


Fig. 1 XRD patterns of the typical CuO straw sheaves

3. Results and discussion

3.1 Characterization of the typical CuO straw sheaves

Fig. 1 shows the XRD patterns of the typical straw sheaf-like CuO sample. All the diffraction peaks well agree with the standard card (JCPDS file no.05-0661). No impurities peaks, such as Cu_2O and $\text{Cu}(\text{OH})_2$, can be detected in the XRD patterns, indicating the formation of phase-pure monoclinic CuO. It is worth noting that the intensity ratio of $\{002\}$ to $\{110\}$ peaks is 20.5 for the CuO straw sheaves (Fig. S1 of ESI[†]), which is greatly higher than that (9.7) of bulk CuO, indicating that the $\{002\}$ facets preferentially grow. This will be further demonstrated by HRTEM and SEAD in the latter part.

Fig. 2 shows the typical SEM images of the sample. It is clear that the sample presents the uniform and well-defined straw sheaf-like microstructures consisting of the microrods. The individual straw sheaf has a size of $(40\text{-}50)\ \mu\text{m} \times (5\text{-}6)\ \mu\text{m}$ (Fig. 2a). Fig. 2b reveals that an obvious splitting seems to occur in the middle of straw sheaf. Viewed along the axial direction, the end of the straw shows the fantail-like structure, and the single microrod shows a rectangle cross-section of $(0.8\text{-}1.5)\ \mu\text{m} \times (0.6\text{-}1)\ \mu\text{m}$. (Fig. 2c). Further viewed along the radial direction, the straw fantail consists of the outspread micron bundles, of which the microrods have a clean and smooth surface, on which no nanoparticles attached (Fig. 2d).

HRTEM is conducted to further observe the structure of the sample. In Fig 3a, the side and the top or end of the individual microrod can be identified clearly, marked with the white dotted line. The single crystalline nature of the sample can be revealed by the SAED pattern, which is performed along the $[001]$ zone axis (the inset of Fig 3a). The clear diffraction spots can be identified as the (110) , (010) and (100) planes of the monoclinic CuO^[30]. To the best of our knowledge, it is the first time to synthesize the single-crystalline CuO straw sheaves by a simple method. To identify the structure of the microrod more exactly, the lattice fringe images are further observed in Regions 1 and 2, which are marked with red and blue rectangles. In Fig 3b, the interplanar spacing is 0.25 nm, corresponding to the (002) plane of monoclinic CuO. In Fig 3c, the lattice spacing is 0.28 nm, which correspond to the (110) plane. Combining with the XRD results, it can be demonstrated that the microrod grow

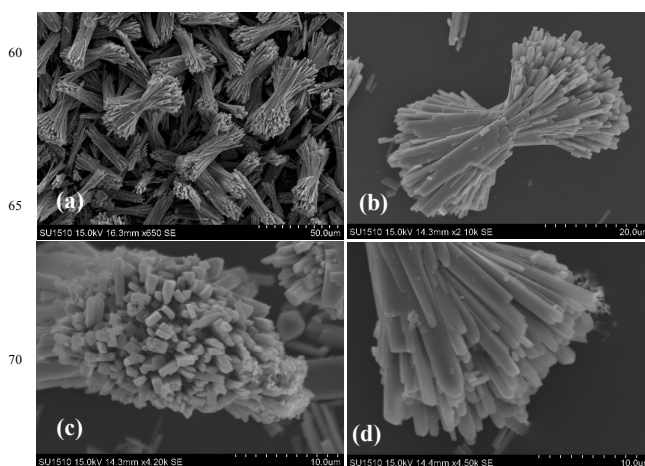


Fig. 2 SEM images of the typical CuO straw sheaves observed (a,b) at different magnifications and (c,d) along different directions

preferentially along the $[001]$ direction. Furthermore, we could conclude that the side and end surfaces of the microrod are composed of the $\{110\}$ and the $\{002\}$ facets, respectively (Fig. 3d). We have calculated the percentage of the exposed $\{110\}$ facets is 69.91% on base of its geometric shapes. It is clear that the sample exposes a high-percentage $\{110\}$ facets.

3.2 Influences of the added amount of Cu(II) ion

It has been reported^[31-37] that crystal splitting is associated with the fast crystal growth rate that is strongly dependent on the supersaturation of solution. As a result, the change of Cu^{2+} concentration may result in the different degree splitting of CuO crystals. The effect of Cu^{2+} concentration on the samples are mainly investigated while keeping the others experimental parameters constant. At a low amount of CuSO_4 added (7.8 mmol), the as-prepared sample consists of uniform and well-defined flowers with the diameters of about 10-15 μm (Fig 4a). At a high magnification (Fig 4b), it is observed that the petal of the flowers show a triangular shape, and the petals are about 100-300 nm thick. While the amount of CuSO_4 is increased to 15.6

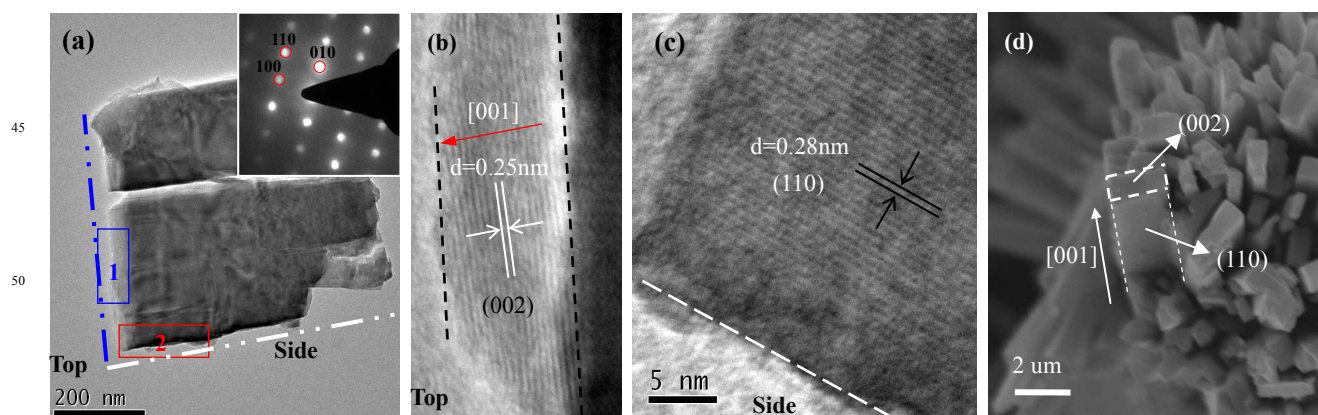


Fig. 3 HRTEM and SEM micrographs of the typical CuO straw sheaves: (a) HRTEM (the inset of ED patterns); (b) Lattice fringe image of the nanorod top marked with Rectangle 1; (c) Lattice fringe image of the nanorod side marked with Rectangle 2; (d) SEM

Cite this: DOI: 10.1039/c0xx00000x

www.rsc.org/xxxxxx

ARTICLE

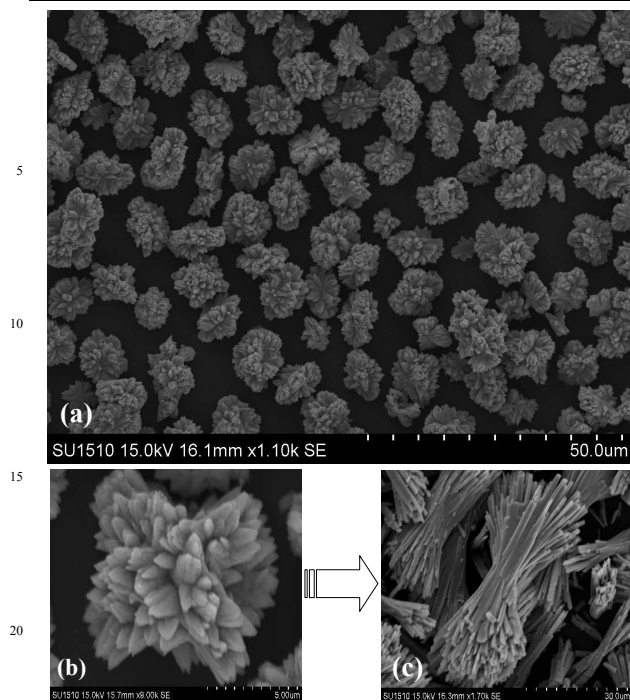


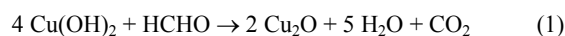
Fig. 4 Effect of the added amount of Cu(II) ion on the samples: (a,b) 7.8 mmol (c) 15.6 mmol

mmol, the straw sheaves are obtained (Fig. 4c). It seems that the copper ion (II) concentration has an important influence on the shapes and sizes of CuO sample, and that the straw sheaves evolve from the splitting growth of the flowers. It has been reported^[34] that crystal splitting, which is unique to minerals in nature, occurs only at a certain critical level of the supersaturation. According to the classical crystallography theory^[38], a large number of nuclei burst out rapidly at a high concentration of Cu²⁺. Generally, a lower monomer concentration favors isotropic growth, while a higher monomer concentration favors anisotropic growth^[38]. Therefore, the flowers form at a lower concentration while the straw sheaves form at a higher concentration.

3.3 Influences of reaction temperature and the HMT amount

The temperature-dependent experiments have been performed to investigate the effect of reaction temperature on the samples. At 80 and 100 °C, the irregular sample form (Fig. S2(a,b) of ESI^{*}). The novel straw sheaves form only at 120 °C (Fig. S2c of ESI^{*}). Further increasing the reaction temperature to 140 °C, nevertheless, the irregular sample form and also a significant amount of Cu₂O form (Figs. S2d and S3 of ESI^{*}). We hold that the microstructure variation caused by temperature is mainly driven kinetically. It has been reported that^[32] the splitting of crystal is most dependent on the solute supersaturation and/or the impurities concentrations in solution, which usually change significantly in the microenvironment of crystal growth. At low

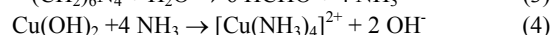
temperatures, ammonia molecules, as an impurity, will be released slowly by the hydrolysis of HMT, indicated by the low pH values (6-7) of the system. At high temperatures, more ammonia molecules are released by the rapid hydrolysis of HMTs, and a large number of nuclei burst out rapidly in a short time and grow fast; at the same time, more ammonia molecules released may adsorb on the crystals surfaces; As a result, the adsorbed ammonia molecules could lead to the crystal splitting growth^[32]. This needs further research. Wang et al. have reported that HMT can control the morphology of crystals^[39,40]. On the other hand, more formaldehyde molecules are produced at higher temperatures by the hydrolysis of HMT; As a result, the formed Cu(OH)₂ can be reduced to Cu₂O, as described by Equation (1) as follows.

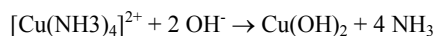


Furthermore, the effect of the HMT/Cu(II) molar ratios has been investigated at 5, 10 and 15 (Fig. S4 of ESI^{*}). At 5 and 10, the CuO straw sheaves consist of the compact microrods; at 15, the particles with Cu₂O octahedrons form due to the formation of many HCHO molecules, by which Cu(II) ions have been reduced to Cu(I) ions. In the absence of HMT, only short and thick microrods form (Fig. S5 of ESI^{*}), but the unknown impurities phases form (not showing). Summarily, the morphology and phase composition of the sample is affected by the amount of HMT added.

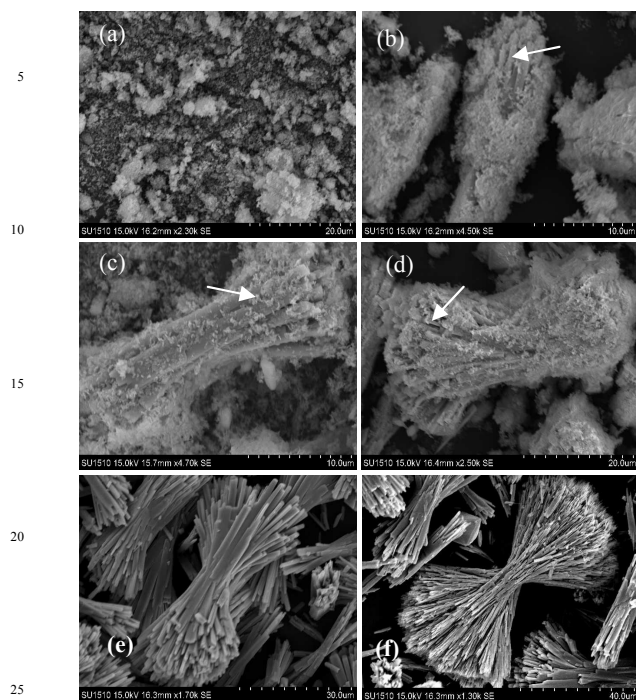
3.4 Growth Mechanism of CuO straw sheaves

In order to understand the formation of CuO straw sheaves, the time-dependent experiments are carried out, while keeping other reaction parameters constant. Fig. 5A shows the morphology evolution from 6 h to 31 h. In the initial time, the nano or microparticles form, and aggregate to form large particles and then the nanorods form from inner of the large particles. It seems that straw sheaves have formed at the early stage. With the increase of time, the straw sheaves continuously to grow, and both ends of the straw sheave become larger. Hence a crystal splitting mechanism is proposed to understand its formation^[31-37]. Fig 5B presents the schematic diagram of splitting growth. The numerous nanocrystals form large crystals; the large crystals further splitting grow to form the straw sheaf. Such crystal splitting growth way is a common growth phenomenon for some minerals in nature, which has been also noticed in other crystals, such as Ce(1,3,5-BTC)(H₂O)₆^[31], Bi₂S₃^[32], La(1,3,5-BTC)(H₂O)₆^[33], and so on. Moreover, it is reported that crystal splitting is closely relative to the fast crystal growth velocity that is dependent on the solution supersaturation^[34]. In our synthesis, there may exist the chemical reactions as follows.





(A)



(B)

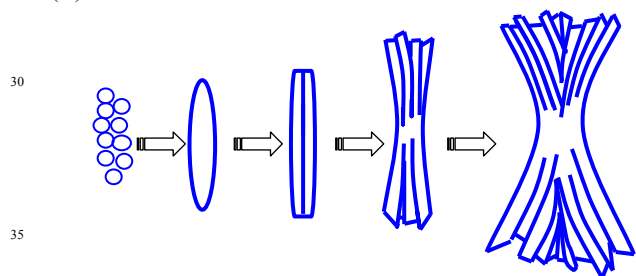
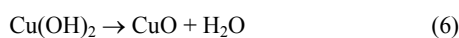


Fig. 5 (A) SEM images of the samples prepared at different reaction times: (a) 6 h, (b) 14 h, (c) 16 h, (d) 20 h, (e) 24 h, (f) 31 h; (B) Schematic growth diagram of the straw sheaves



It has been reported methenamine would hydrolyze to produce OH^- , NH_3 and HCHO under hydrothermal conditions [41,42]. On one hand, the stability constant (K_f) of $[\text{Cu}(\text{NH}_3)_4]^{2+}$ is 2.1×10^{13} , so NH_3 can complex with Cu^{2+} ions to form $[\text{Cu}(\text{NH}_3)_4]^{2+}$ [43]. On the other hand, the solubility product (K_{sp}) of $\text{Cu}(\text{OH})_2$ is 4.8×10^{-20} , so the Cu^{2+} ions in the $[\text{Cu}(\text{NH}_3)_4]^{2+}$ complex can be released slowly under hydrothermal conditions. While the released OH^- reach a high concentration enough, the OH^- will combine with the released Cu^{2+} to form $\text{Cu}(\text{OH})_2$; then $\text{Cu}(\text{OH})_2$ converts to CuO after calcination. There is a competitive reaction among the chemical species. Therefore, we hold that methenamine mainly provide NH_3 and OH^- , which control the formation of $\text{Cu}(\text{OH})_2$. Furthermore, it has been reported that the extra ammonia molecules can insert into the layers of crystallographic network [34]. Because of the strong adhesion of ammonia molecules to the newly created surface [32], the growth of the crystal may distort,

60 resulting in the crystal splitting. To conclude, the formed ammonia molecules may

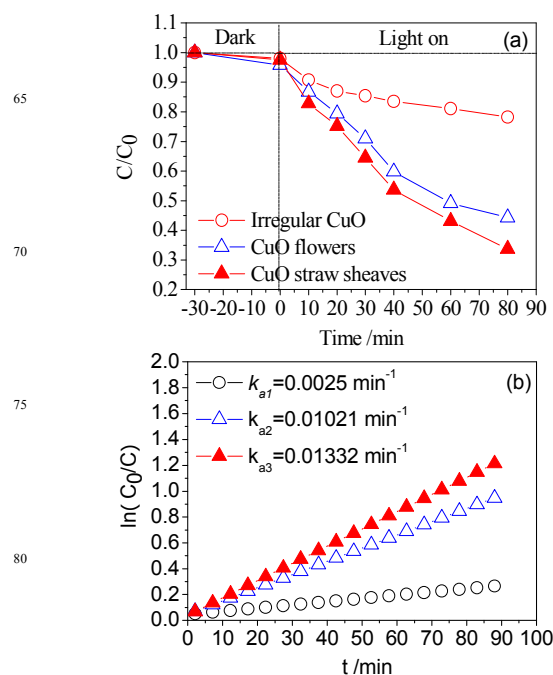


Fig. 6 (a) Degradation curves and (b) apparent reaction kinetics curves of the samples for the degradation of RhB under visible light irradiation ($\lambda \geq 420 \text{ nm}$): k_{a1} , k_{a2} and k_{a3} , apparent reaction rate constants for irregular CuO, CuO flowers and CuO straw sheaves, respectively; (c) Super cell model; (d) Atomic configuration of the (110) facet

play an important role in the formation of straw sheaves, Hence, we believe that the splitting mechanism may more appropriately account for straw sheaf-like CuO.

115 3.5 Photocatalytic properties

Fig 6a and b show the photodegradation curves and the apparent rate constants of the CuO samples for the degradation of RhB dye

under visible-light irradiation ($\lambda \geq 420$ nm), respectively. The CuO straw sheaves exhibit a higher photocatalytic activity than the two latters. The apparent rate constant (k_a) of the CuO straw sheaves is 5.3 and 1.3 times higher than those of the irregular and flower-like CuO samples, respectively. Fig. S6 (ESI[†]) shows that after 140-min irradiation, about 24.5% of RhB are mineralized by CuO straw sheaves. In order to understand their different activities, the surface areas and crystallinities of the samples are mainly investigated (Table S1 and Fig. S7 of ESI[†]). The BET areas of the irregular CuO, the CuO flowers and the CuO straw sheaves are 27.0, 28.5 and 21.8 m²/g, respectively. Although the former two samples have higher BET areas than the latter, their crystallinities (41.7% and 57.7%) are lower than that (75.9%) of the latters (Table S1 of ESI[†]). The low crystallinity suggests a more defects [44]. It is reported that the bulk defects of photocatalysts are usually considered to be the recombination centers for electrons and holes [44], resulting in a low photocatalytic activity. Therefore, the lower activities of the former two samples are attributed to their lower crystallinities. Furthermore, the facet effect is also considered. The CuO straw sheaves have the 66.9% of the {110} facets exposed. However it is difficult to determine the exposed facets of CuO flowers due to its compact structures. (Fig. S8 of ESI[†]). Observed from Fig. 6 (c,d), Fig. S9 and Table S2 (ESI[†]), the atom density on (110) facet is higher than those of (200), (002) and (111) or (-111) facets. Herein, we can only assume that the exposed {110} facets play an important role, which needs extensive research. The copper (II) ions in the {110} planes can accept more photogenerated electrons by visible-light irradiation. As a result, the formed copper (I) atomic layers favor for the separation of the electron-hole pairs [45]. Besides, the copper (I) ions will result in the oxygen vacancies neighboring copper (I) ions, which will increase the photocatalytic active sites [45]. Furthermore, the photoresponses of the CuO electrodes have been measured and the results are shown in Fig. S10 (ESI[†]). The photocurrent of CuO straw sheaves electrode is the highest than those of irregular and flower-like ones under visible light irradiation. The improved photocurrent of CuO straw sheaves electrode may originate from an enhanced charge separation, which benefits to the improved photocatalytic properties. Summarily, the high crystallinity and the active {110} facets exposed of CuO straw sheaves, instead of its BET area, play the crucial roles in improving the photoactivity.

4. Conclusions

The novel single-crystalline CuO straw sheaves can be prepared through a facile two-step process, which is mainly maneuvered by the precursors concentrations, temperature and the HMT amount added. The CuO straw sheaves have a high photocatalytic activity, which has been attributed to the high crystallinity and the high-proportion {110} facets exposed.

Acknowledgements

This work is financially supported by National Science Foundation of China (21377060, 21103049), Six Talent Climax Foundation of Jiangsu (20100292), Jiangsu Science Foundation of China (BK2012862), Jiangsu Province of Academic Scientific Research Industrialization Projects (JHB2012-10, JH10-17), The Project of Foreign Culture and Education expert (N0502001003), Jiangsu province of Key Environmental protection projects (2012028), Teaching Reform Project to Enhance the Practice Innovation of NUIST-2013 (N1885013014), Support Program for Undergraduate Dissertation of NUIST-2013 (N1085002008), A

Project Funded by the Priority Academic Program Development of Jiangsu Higher Education Institutions (PAPD), and Jiangsu Province Innovation Platform for Superiority Subject of Environmental Science and Engineering, "333" Outstanding Youth Scientist Foundation of Jiangsu (2011-2015), the Project Sponsored by SRF for ROCS, SEM (2013S002).

Notes and references

Jiangsu Key Laboratory of Atmospheric Environment Monitoring and Pollution Control, Innovative Research Laboratory of Environment and Energy, School of Environmental Sciences and Engineering, Nanjing University of Information Sciences and Engineering, Nanjing 210044, China. Corresponding author. Email: tfwd@163.com (F. Teng); Phone: 86-25-58731090

† Electronic Supplementary Information (ESI[†]) available: Peaks intensity ratios of CuO straw sheaves, SEM images and XRD patterns of the samples at different temperatures, SEM images of the samples at different molar ratios of HMT /Cu²⁺, SEM images of the sample prepared without adding HMT, XRD patterns, BET areas and crystallinity of the samples, are freely available over <http://www.rsc.com>

- (a) J. T. Hu, T. W. Odom and C. M. Lieber, *Acc. Chem. Res.*, 1999, **32**, 435. (b) G. R. Patzke, F. Krumeich and R. Nesper, *Angew. Chem., Int. Ed.*, 2002, **41**, 2446. (c) Y. Xia, P. Yang, Y. Sun, Y. Wu, B. Mayers, B. Gates, Y. Yin, F. Kim and Y. Yan, *Adv. Mater.*, 2003, **15**, 353. (d) C. N. R. Rao, F. L. Deepak, G. Gundiah and A. Govindaraj, *Prog. Solid State Chem.*, 2003, **31**, 5.
- W. Zhao, F. Gonzaga, Y. Li and M. A. Brook, *Adv. Mater.*, 2007, **19**, 1766.
- M. Sevilla, S. Alvarez and A. B. Fuertes, *Micropr. Mesopr. Mater.*, 2004, **74**, 49.
- Y. Zheng, C. Chen, Y. Zhan, X. Lin, Q. Zheng, K. Wei, J. Zhu and Y. Zhu, *Inorg. Chem.*, 2007, **46**, 6675.
- J. Zhang, H. Liu, Z. Wang and N. Ming, *Appl. Phys. Lett.*, 2007, **91**, 133112.
- L. Kang, Z. Wang, Z. Cao, Y. Ma, H. Fu and J. Yao, *J. Am. Chem. Soc.*, 2007, **129**, 7305
- (a) Y. Wu, J. Yang, G. C. Han, B. Y. Zong, H. Q. Ni, P. T. Luo, C. Chong, T. S. Low and Z. X. Shen, *Adv. Funct. Mater.*, 2002, **12**, 489. (b) L. Vayssieres, N. Beermann, S. E. Lindquist and A. Hagfeldt, *Chem. Mater.*, 2001, **13**, 233. (c) A. Hatzor and P. S. Weiss, *Science*, 2001, **291**, 1019. (d) M. Li, H. Schnablegger and S. Mann, *Nature*, 1999, **402**, 393. (e) Z. Zhang, G. Ramanath, P. M. Ajavan, D. Goldberg and Y. Bando, *Adv. Mater.*, 2001, **13**, 197. (f) J. K. N. Mbindyo, B. D. Reiss, B. R. Martin, C. D. Keating, M. J. Natan and T. E. Mallouk, *Adv. Mater.*, 2001, **13**, 249.
- M. Vaseem, A. Umar, Y. B. Hahn, D. H. Kim, K. S. Lee, J. S. Jang and J. S. Lee, *Catal. Commun.*, 2008, **10**, 11.
- J. M. Hong, J. Li and Y. H. Ni, *J. Alloys Compd.*, 2009, **481**, 610.
- S. L. Wang, H. Xu, L. Q. Qian, X. Jia, J. W. Wang, Y. Y. Liu and W. H. Tang, *J. Solid State Chem.*, 2009, **182**, 1088.
- J. Zhang, J. Liu, Q. Peng, X. Wang and Y. Li, *Chem. Mater.*, 2006, **18**, 867.
- X. P. Gao, J. L. Bao, G. L. Pan, H. Y. Zhu, P. X. Huang, F. Wu and D. Y. Song, *J. Phys. Chem. B*, 2004, **108**, 5547.
- G. Zou, H. Li, D. Xiong, K. Zhang, C. Dong and Y. Qian, *J. Phys. Chem. B*, 2006, **110**, 1632.
- (a) C. T. Hsieh, J. M. Chen, H. H. Lin and H. C. Shih, *Appl. Phys. Lett.*, 2003, **83**, 3383. (b) J. Chen, S. Deng, N. Xu, W. Zhang, X. Wen and S. Yang, *Appl. Phys. Lett.*, 2003, **83**, 746.
- Y. Sun and Y. Xia, *Science*, 2002, **298**, 2176.
- T. S. Ahmadi, Z. L. Wang, T. C. Green, A. Henglein and M. A. El-Sayed, *Science*, 1996, **272**, 1924.
- B. J. Wiley, Y. Xiong, Z. Y. Li, Y. Yin and Y. Xia, *Nano Lett.*, 2006, **6**, 765.
- C. Burda, X. Chen, R. Narayanan and M. A. El-Sayed, *Chem. Rev.*, 2005, **105**, 1025.

19. P. Jiang, S. Y. Li, S. S. Xie, Y. Gao and L. Song, *Chem.-Eur. J.*, 2004, **10**, 4817.
20. A. Tao, F. Kim, C. Hess, J. Goldberger, R. He, Y. Sun, Y. Xia and P. Yang, *Nano Lett.*, 2003, **3**, 1229.
- 5 21. Y. Chang, M. L. Lye and H. C. Zeng, *Langmuir*, 2005, **21**, 3746.
22. R. Jin, Y. Cao, C. A. Mirkin, K. L. Kelly, G. C. Schatz and J. G. Zheng, *Science*, 2001, **294**, 1901.
23. M. Maillard, S. Giorgio and M. P. Pileni, *Adv. Mater.*, 2002, **14**, 1084.
- 10 24. Y. Sun and Y. Xia, *Adv. Mater.*, 2003, **15**, 695.
25. F. Dumestre, B. Chaudret, C. Amiens, M. C. Fromen, M. J. Casanove, P. Renaud and P. Zurcher, *Angew. Chem., Int. Ed.*, 2002, **41**, 4286.
26. (a) W. X. Zhang, X. G. Wen and S. H. Yang, *Inorg. Chem.*, 2003, **42**, 5005. (b) H. W. Hou, Y. Xie and, Q. Li, *Cryst. Growth Des.*, 2005, **5**, 201. (c) Y. Y. Xu, D. R. Chen and X. L. Jiao, *J. Phys. Chem. B*, 2005, **109**, 13561.
- 15 27. C. T. Hsieh, J. M. Chen, H. H. Lin and H. C. Shih, *Appl. Phys. Lett.*, 2003, **82**, 3316.
- 20 28. B. Liu and H. C. Zeng, *J. Am. Chem. Soc.*, 2004, **126**, 8124.
29. X. G. Wen, W. X. Zhang and S. H. Yang, *Langmuir*, 2003, **19**, 5898.
30. L. C. Wang, W. Gong, H. Wang, C. D. Wang, K. Tang and Y Qian, *J. Mater. Chem.*, 2012, **22**, 11297.
- 25 31. K. Liu, H.P. You and G. Jia, *Cryst. Growth Des.*, 2010, **10**, 790.
32. J. Tang and A.P. Alivisatos, *Nano Lett.*, 2006, **6**, 2701.
33. K. Liu, Y.H. Zheng and G. Jia, *J. Solid State Chem.*, 2010, **183**, 2309.
34. P. Punin and O. Yu, *Crystal Splitting. Zap. Vses. Mineral. Ova. part 110*, No. 6, 666-686 (Russian).
- 30 35. C.H. Lu, L. M. Qi, J. H. Yang, X. Y. Wang, D. Y. Zhang, J. L. Xie and J. M. Ma, *Adv. Mater.*, 2005, **17**, 2562.
36. H. R. Zhang, C. M. Shen, S. T. Chen, Z. H. Xu, F. S. Liu, J. Q. Li and H. J. Gao, *Nanotechnology*, 2005, **16**, 267.
- 35 37. J. P. Yang, F. C. Meldrum and J. H. Fendler, *J. Phys. Chem.*, 1995, **99**, 5500.
38. T.-D. Nguyen and T.-O. Do, *J. Phys. Chem. C*, 2009, **113**, 11204
39. V. Mohammad, U. Ahmad, H. K. Sang and H. Yoon-Bong, *J. Phys. Chem. C*, 2008, **112**, 5729.
- 40 40. H. Wang, C. Xie, D. Zeng and Z. J. Yang, *Colloid Interface Sci.*, 2006, **297**, 570.
41. K. Govender, D.S. Boyle, P.B. Kenway and P.O. Brien, *J. Mater. Chem.*, 2004, **14**, 2575.
42. J.G. Strom Jr. and H.W. Jun *J. Pharm. Sci.*, 1980, **69**, 1261.
- 45 43. Y.G. Zhang, S.T. Wang, Y.T. Qian and Z.D. Zhang, *Solid State Sci.*, 2006, **8**, 462.
44. 41B. Ohtani, *J. Photochem. Photobio. C*, 2010, **11**, 157.
45. 42H. Hu, Z. Jiao, H. Yu, G. Lu, J. Ye and Y. Bi, *J. Mater. Chem.*, 2013, **1**, 2387.